Spectrochimica Acta Part A 89 (2012) 168–176

Contents lists available at SciVerse ScienceDirect

Spectrochimica Acta Part A: Molecular and Biomolecular Spectroscopy

journal homepage: www.elsevier.com/locate/saa

Physicochemical studies of chemosensor imidazole derivatives: DFT based ESIPT process

Jayaraman Jayabharathi*, Venugopal Thanikachalam, Karunamoorthy Jayamoorthy

Department of Chemistry, Annamalai University, Annamalainagar, Tamilnadu 608 002, India

ARTICLE INFO

Article history:
Received 20 October 2011
Received in revised form 9 December 2011
Accepted 21 December 2011

Keywords:
Greenway synthesis
NLO
HOMO–LUMO
MEP
Chemosensor

ABSTRACT

A series of substituted imidazoles have been synthesized in very good yield under a solvent free condition using molecular iodine as the catalyst. An excited state intramolecular proton transfer (ESIPT) process in hydroxy imidazole has been studied using emission spectroscopy. DFT calculations on energy, dipole moment, charge distribution of the rotamers in the ground and excited states of the imidazole derivatives have been performed and discussed. DFT analysis about HOMO, HOMO−1, LUMO and LUMO+1 has been carried out and discussed. The energy barrier for the interconversion of two rotamers is too high in the excited state than the ground state that is shown by PES calculation. The molecular electrostatic potential surface (MEP) has also been employed to show the higher electron density at N(3) nitrogen. Fluorescence enhancement has been found in the presence of transition metal ions and this may result from the suppression of radiationless transitions from the n–π* state in the chemosensors.

1. Introduction

Excited state intramolecular proton transfer (ESIPT) phenomena have been investigated [1,2] due to the practical applications of ESIPT exhibiting molecules used as laser dyes, photo stabilizers, fluorescent probes in biology and light-emitting materials for electroluminescent devices [2–4]. ESIPT occurs in molecules having a phenolic hydroxy group with an intramolecular hydrogen bond to the nearby hetero atom of the same chromophore. The proton in the hydroxy group upon photo excitation migrates to the hetero atom at a distance <2 Å to form the excited state tautomer. The ESIPT exhibiting substances have dual fluorescence, depending on the molecular nature and external factors such as solvent polarity and temperature.

Organic solvents are high on the list of damaging chemicals, so designing of "green" experimental protocol is a challenge to chemists to improve the quality of synthesis. Though there are several methods reported in the literature [5–8] for the synthesis of imidazoles, they suffer from disadvantages such as harsh reaction conditions, poor yields, prolonged time period, use of hazardous and expensive acid catalysts. The advantages associated with eco-friendly iodine element, has been explored as a powerful catalyst for various syntheses [9]. During the course of our studies towards the development of new route to the synthesis, we wish to report a simple and efficient method for the synthesis of substituted imidazoles. Herein we focus light on the photophysical studies of 2-arylimidazole derivatives (**1**–**4**) and ESIPT process of hydroxy imidazole **3**. Density functional theory (DFT) calculation [10] on energy, dipole moment of various species, HOMO, HOMO−1, LUMO and LUMO+1 energies, PES and molecular electrostatic potential surface (MEP) studies have been performed and discussed.

2. Experimental

2.1. Optical measurements and composition analysis

NMR spectra have been recorded for the 2-arylimidazole derivatives (**1**–**4**) on a Bruker 400 MHz instrument. The ultraviolet–visible (UV–Vis) spectra have been measured on UV–Vis spectrophotometer (Perkin Elmer, Lambda 35) and corrected for background due to solvent absorption. Photoluminescence (PL) spectra have been recorded on a (Perkin Elmer LS55) fluorescence spectrometer. Solvents used for spectral measurements are spectroscopic grade. Mass spectra have also been recorded on a Varian Saturn 2200 GCMS spectrometer. The fluorescence quantum yield has been measured in acetonitrile using coumarin 47 as a standard [11] according to the equation, $\Phi_{unk} = \Phi_{std}(I_{unk}/I_{std})(A_{std}/A_{unk})(\eta_{unk}/\eta_{std})^2$, where Φ_{unk}, Φ_{std}, I_{unk}, I_{std}, A_{unk}, Φ_{unk} and Φ_{std} are the fluorescence quantum yields, the integration of the emission intensities, the absorbances at the excitation wavelength and the refractive indexes of the corresponding solution of the 2-aryl imidazole derivatives (**1**–**4**) and the standard, respectively. The radiative (k_r) [$k_r = \Phi_p/\tau$] and non-radiative (k_{nr})

* Corresponding author. Tel.: +91 9443940735.
E-mail address: jtchalam2005@yahoo.co.in (J. Jayabharathi).

1386-1425/$ – see front matter © 2012 Elsevier B.V. All rights reserved.
doi:10.1016/j.saa.2011.12.053

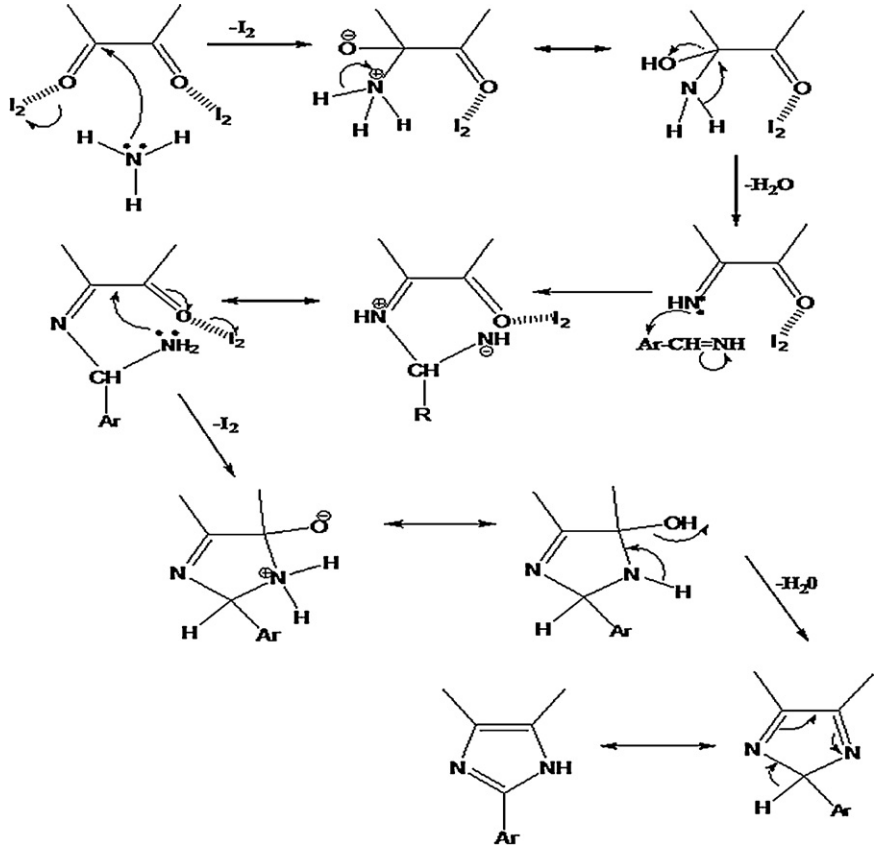

Scheme 1. Experimental pathway for the synthesis of imidazole derivatives **1**–**4**.

$[k_{nr} = 1/\tau - \Phi_p/\tau]$ rate constants were calculated using the life time (τ) of the excited state.

2.2. Molecular electrostatic potential (MEP) calculation

In the present work MEPs derive from a classical point charge model. The electrostatic potential for each molecule is obtained by moving a unit positive point charge across the van der Waals surface and it is calculated [12] at various points j on this surface using, $V_j = \sum q_i/r_{ji}$, where q_i represents the partial charge of each atom i, and r_{ji} is the distance between point's j and atom i. Starting from the 3D model of a molecule and its partial atomic charges, the electrostatic potential is calculated for points on the molecular surface.

2.3. Synthesis of 2-arylimidazole derivatives (*1*–*4*)

The greenway experimental pathway [13] used for the synthetic mechanism of 2-aryl imidazole derivatives (**1**–**4**) has been given in Scheme 1.

2.3.1. 2,4,5-Triphenyl-1H-imidazole (*1*)

A mixture of benzaldehyde (1 mmol), benzil (1 mmol), ammonium acetate (2.5 mmol) and iodine (15 mol%) were grined in a morter at room temperature for appropriate time. The reaction was monitored by TLC and the reaction mixture was treated with aqueous $Na_2S_2O_3$, the formed crude was purified by column chromatography using *n*-hexane:ethyl acetate (9:1) as the eluent. Yield: 60%. mp = 121 °C, Anal. calcd. for $C_{22}H_{16}N_2$: C, 85.11; H, 5.44; N, 9.45. Found: C, 84.92; H, 5.39; N, 9.69. ^{1}H NMR (400 MHz, $CDCl_3$): δ 7.23–8.10 (m, 15H), 12.66 (s, 1H). ^{13}C (100 MHz, $CDCl_3$): δ 125.67, 126.96, 127.54, 128.23, 128.63–129.13, 130.84, 131.58, 135.68, 137.60, 145.96 (aromatic carbons). MS: *m*/*e* 296.37, calcd 297.37 [M+1].

2.3.2. 2-(2,4-Difluorophenyl)-4,5-diphenyl-1H-imidazole (*2*)

A mixture of 2,4-difluorobenzaldehyde (1 mmol), benzil (1 mmol), ammonium acetate (2.5 mmol) and iodine (15 mol%) were grined in a morter at room temperature for appropriate time. The reaction was monitored by TLC and the reaction mixture was treated with aqueous $Na_2S_2O_3$; the formed crude was purified by column chromatography using *n*-hexane:ethyl acetate (9:1) as the eluent. Yield: 55%. mp = 167 °C, Anal. calcd. for $C_{21}H_{14}F_2N_2$: C, 75.89; H, 4.25; N, 8.43. Found: C, 75.05; H, 4.14; N, 7.10. ^{1}H NMR (400 MHz, $CDCl_3$): δ 7.23–8.14 (m, 13H), 12.67 (s, 1H). ^{13}C (100 MHz, $CDCl_3$): δ 116.02, 116.19, 127.00–129.12 (aromatic carbons), 131.52, 135.59, 137.56, 141.63, 145.15. MS: *m*/*e* 332.05, calcd 333.35 [M+1].

2.3.3. 5-Bromo-2-(4,5-diphenyl-1H-imidazol-2-yl)phenol (*3*)

A mixture of 5-bromo-2-hydroxybenzaldehyde (1 mmol), benzil (1 mmol), ammonium acetate (2.5 mmol) and iodine (15 mol%) were grined in a morter at room temperature for appropriate time. The reaction was monitored by TLC and the reaction mixture was treated with aqueous $Na_2S_2O_3$, the formed crude was purified by column chromatography using *n*-hexane:ethyl acetate (9:1) as the eluent. Yield: 55%. mp = 143 °C, Anal. calcd. for $C_{21}H_{15}BrN_2O$: C, 64.46; H, 3.86; N, 7.16. C, 64.96; H, 3.95; N, 7.61. ^{1}H NMR (400 MHz, $CDCl_3$): δ 6.93–8.05 (m, 13H), 12.97 (s, 2H). ^{13}C (100 MHz, $CDCl_3$): δ 113.36–130.54 (aromatic carbons), 146.33, 157.17. MS: *m*/*e* 390.00, calcd 391.26 [M+1].

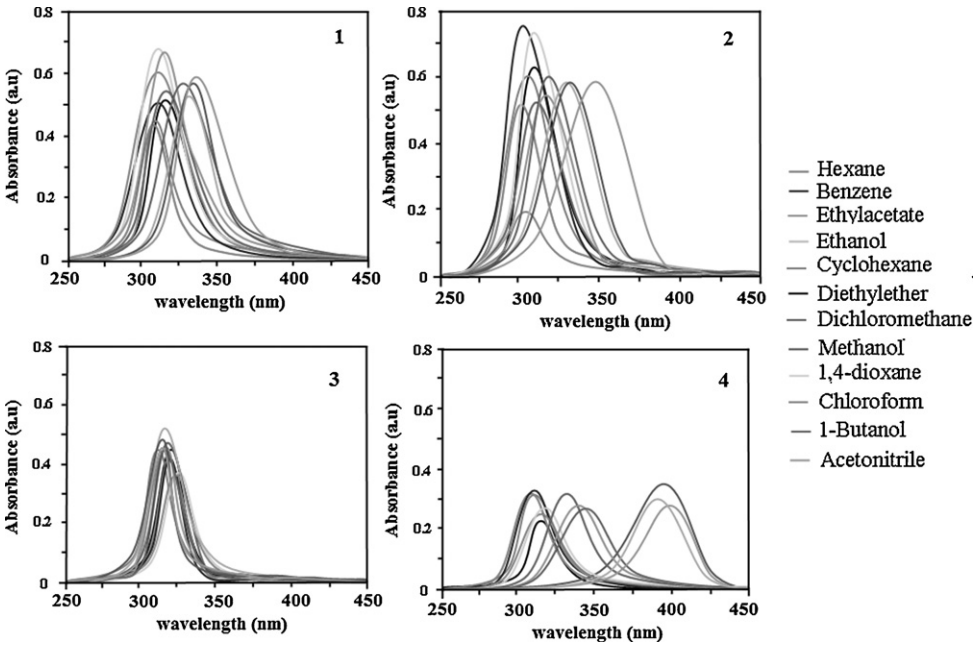

Fig. 1. Excitation spectra of the imidazole derivatives **1**–**4**.

*2.3.4. 2-(2-Methoxyphenyl)-4,5-diphenyl-1H-imidazole (**4**)*

A mixture of 2-methoxybenzaldehyde (1 mmol), benzil (1 mmol), ammonium acetate (2.5 mmol) and iodine (15 mol%) were grined in a morter at room temperature for appropriate time. The reaction was monitored by TLC and the reaction mixture was treated with aqueous $Na_2S_2O_3$, the formed crude was purified by column chromatography using *n*-hexane:ethyl acetate (9:1) as the eluent. Yield: 50%. mp = 178 °C, Anal. calcd. for $C_{22}H_{18}N_2O$: C, 80.96; H, 5.56; N, 8.58. Found: C, 80.00; H, 5.06; N, 8.41. ^{1}H NMR (400 MHz, $CDCl_3$): δ 3.87 (s,3H), 6.97–7.87 (m, 14H), 12.67 (s, 1H). ^{13}C (100 MHz, $CDCl_3$): δ 55.37, 114.31, 127.79, 126.76–132.45 (aromatic carbons), 146.10, 160.20, 167.30. MS: *m*/*e* 327.50, calcd 327.39 [M+1].

3. Results and discussion

The 2-arylimidazole derivatives (**1**–**4**) fluoresce strongly in solutions at room temperature. Their luminescence excitations spectra (Fig. 1) are in coincidence with their absorption spectra and differ from their emission spectra (Fig. 2). Hence, the fluorescence of the 2-arylimidazole derivatives deserves for discussion. Fluorescence band maxima (λ_{flu}) fluorescence excitation maxima (λ_{exc}) and Stokes shifts ($\Delta\upsilon_{ss}$) have been presented in Table 1. The fluorescence spectra of **3** in dioxane display an abnormal Stokes-shifted emission band at shorter wavelength (410.8 nm) and one small shoulder peak at longer wavelength (460.0 nm). This result shows that in aprotic solvent, the hydroxy 2-arylimidazole exists as two

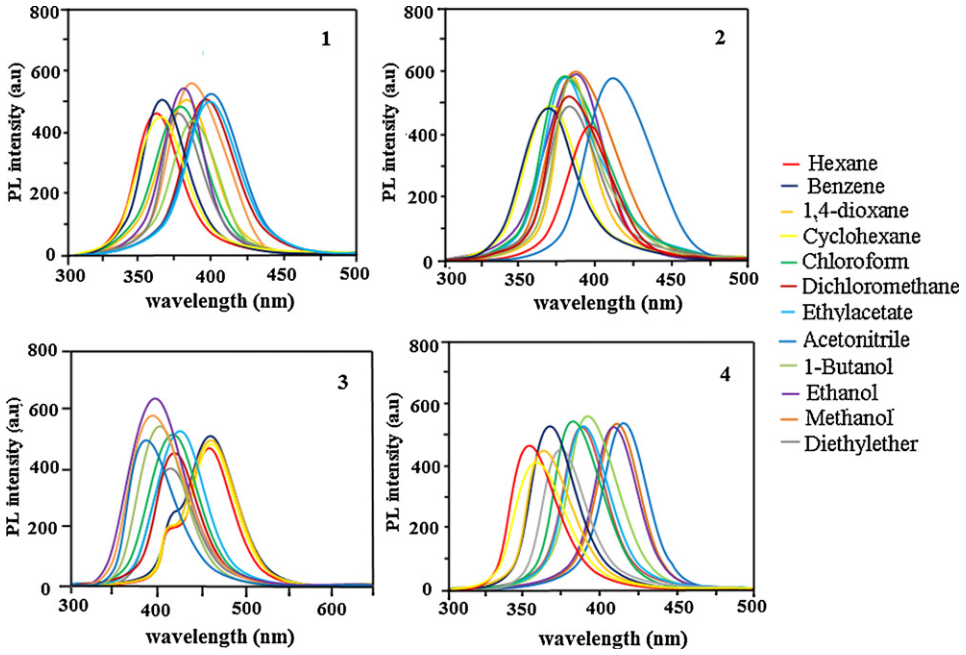

Fig. 2. Emission spectra of the imidazole derivatives **1**–**4**.

Table 1
Photophysical datas of the imidazole derivatives **1**–**4**.

Solvent	**1**			**2**			**3**			**4**		
	λ_{flu}	λ_{exc}	$\Delta\upsilon_{ss}$	λ_{flu}	λ_{exc}	$\Delta\upsilon_{ss}$	λ_{flu}	λ_{exc}	$\Delta\upsilon_{ss}$	λ_{flu}	λ_{exc}	$\Delta\upsilon_{ss}$
Hexane	360.5	309.0	4665	383.4	303.0	7019	409.2, 458.0(sh)	323.2	6503	355.0	308.0	4256
Cyclohexane	365.6	309.6	5000	383.9	304.1	6966	409.9, 459.0(sh)	323.4	6535	360.7	310.4	4576
1,4-dioxane	370.1	310.0	5249	384.2	305.2	6932	410.8, 460.0(sh)	321.0	6588	364.9	311.1	4843
Benzene	375.9	311.2	5418	384.3	306.1	6755	415.3, 462.0(sh)	325.2	6709	370.0	319.8	4390
Diethylether	380.8	314.1	5597	384.9	309.4	6466	417.0, 463.5(sh)	326.5	6760	376.4	320.6	4761
Chloroform	378.1	312.9	5258	385.1	311.2	6197	418.0, 465.0(sh)	327.0	6742	383.8	322.0	5185
Ethyl acetate	381.4	319.0	5011	385.2	316.0	5866	423.2	322.5	7543	388.1	330.1	4555
Dichloromethane	383.5	322.5	5067	386.2	322.0	5279	420.6	320.5	7504	390.6	340.5	3949
1-Butanol	384.3	328.1	4541	386.3	324.5	5042	401.0	319.0	7941	398.7	345.2	3980
Ethanol	388.5	329.1	4526	388.1	341.8	3689	398.2	320.0	8161	419.1	389.7	1728
Methanol	389.2	335.0	4220	397.8	342.5	4239	396.0	322.0	8289	421.8	392.2	1494
Acetonitrile	391.0	337.0	4151	411.9	346.0	4359	429.6	319.0	8139	423.1	397.0	1440

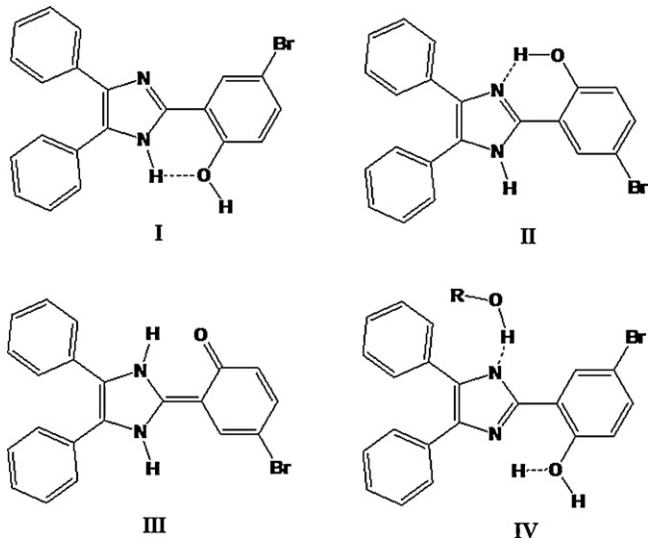

Fig. 3. Intramolecular hydrogen bonded isomeric forms of the imidazole derivative **3**.

different intramolecular hydrogen bonded isomeric forms I and II (Fig. 3). Excitation of the isomer II should lead to the formation of the keto-isomer III due to ESIPT (Fig. 4), while excitation of the isomer I must yield the normal emission. This reveals that only isomer II of these molecules is stable under the experimental conditions. Stokes shift is important for a fluorescent sensor. The higher stokes shift value supplies very low background signals and allows the usage of the material in construction of a fluorescence sensor [13].

However in hydroxylic solvent (EtOH), a short wavelength emission band appears for **3** which is absent in the fluorescence spectra of **1**, **2**, **4** and **5** (Fig. 2). This result corresponds to the data obtained earlier for compounds demonstrating ESIPT [14–16]. This is explained by the presence of intermolecular hydrogen bonding with solvent molecule leading to the stabilization of solvated isomer IV in which ESIPT is impossible.

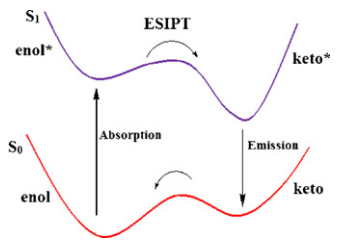

Fig. 4. ESIPT mechanism of the imidazole derivative **3**.

To evidence ESIPT mechanism in **3**, we have performed DFT calculation to know the electron density of the keto and enol isomers of **3** in the ground and the excited states (Table 2). The results reveal that excitation of enol isomer leads to an increase in the electron density at the N(5) nitrogen atom and decreases the same at the oxygen atom resulting in ESIPT. As a consequence of ESIPT, the excited keto isomer is formed. The excited keto isomer emits luminescence and returns to the ground state keto form. This is characterized by a large positive charge at the N(5) nitrogen atom and negative charge at the oxygen atom. As a result, a reverse process occurs in the ground state of the molecule producing the enol form.

3.1. Driving force for ESIPT process

The existence of intramolecular hydrogen bond in hydroxy imidazole **3** is confirmed by the presence of the singlet at 12.97 ppm in the ^{1}H NMR spectra (Fig. 5) which is a typical signal for hydrogen bonded hydrogen atom. In order to reveal the contribution of the intramolecular hydrogen bonding in the hydroxy imidazole **3** to their optical properties, the fluorescence spectra of compound **3** and its methoxy derivative **4** have been measured in dioxane solvent under identical condition (Fig. 6). A dual fluorescence detected for **3** with emission peaks centred at 460 and 410.8 nm, respectively. The emission peak at shorter wavelength (410.8 nm) is assigned to rotamer I and that at the longer wavelength (460 nm) is assigned to rotamer II. Compound **4** exhibits emission peak only at 364.9 nm. The absence of additional peak at longer wavelength confirms the absence of intramolecular hydrogen bond in compound **4**. It is further evident that intramolecular hydrogen bonding is the driving force for ESIPT and the dual fluorescence behaviour of **3**.

3.2. Competition of intra and intermolecular hydrogen bonding in binary solvents

The competition of intra and intermolecular hydrogen bonding in **3** has been studied in dioxane–water mixture. A series of solutions in dioxane–water mixture with different water fraction but identical concentrations of **3** have been made for spectroscopic measurements. In pure dioxane, hydroxy imidazole **3** exhibits both normal and tautomer emission peaks at 410.8 and 460 nm, respectively. The tautomer emission intensity decreases relatively to that

Table 2
Electron density of atoms N(3) oxygen for the imidazole derivative **3**.

Atom	II	II*	III
N(3)	−0.394	−0.456	0.312
O	−0.571	−0.528	−0.698

* Corresponds to excited state of II.

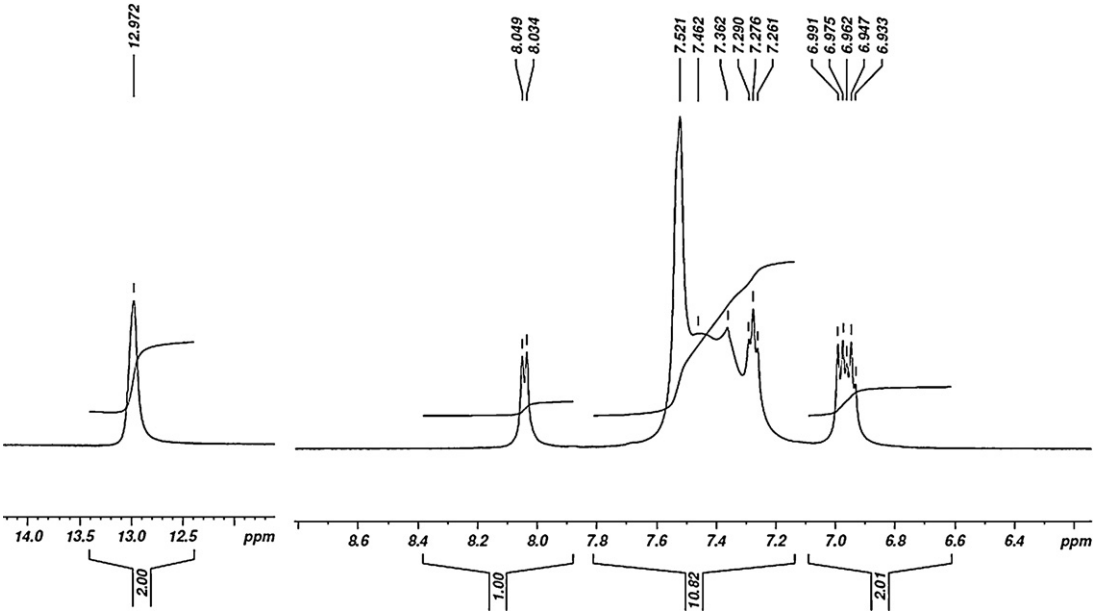

Fig. 5. Expanded ^{1}H NMR spectrum of the imidazole derivative **3**.

of the normal emission with the addition of water. When water fraction is increased to 20% (v/v), the tautomer emission almost vanished. With further increasing water fraction to 40% (v/v), a new emission band appeared at 430.0 nm in addition to the normal emission. This band intensity increased with increasing water fraction and turned to the main emission when water fraction is 80% (v/v) (Fig. 7). It shows that the tautomer emission decreases with increasing water fraction in the mixed solvent if the intermolecular hydrogen bonding between **3** and water is taken into account. In the initial stage, the presence of small amount of water in dioxane solution must give rise to solvation of **3**. The intermolecular hydrogen bonding between **3** and water definitely disrupts the ground state intramolecular hydrogen bonding rotamers I and II but increases the quantity of species IV, in which ESIPT and tautomer formation are inhibited. Consequently the tautomer emission decreases with the addition of water and finally vanished [17].

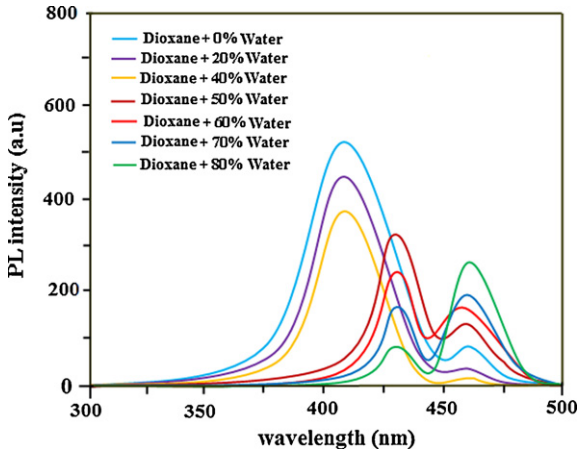

Fig. 7. Competition of intra and intermolecular hydrogen bonding of the imidazole derivative **3** in binary solvents.

3.3. *Density functional theory calculation*

In the present study, theoretical calculations [18–20] have been used to support ESIPT process. The ground-state geometries of the three species, I, II, and III of **3** have been optimized using the DFT/6-31G(d,p) method. The energy of the excited state has also been calculated using the standard CIS method. Table 3 gives the energies and dipole moment of the species I, II, and III in the ground and the excited states. For better understanding the ESIPT mechanism in **3**, we have performed DFT calculation to know the electron density of the keto and enol isomers of **3** in the ground and the excited states (Table 2).

In the excited state the nitrogen atom becomes richer in electrons than the hydroxylic oxygen atom. The π-electron densities in the excited state are the driving force for the intramolecular proton transfer from the hydroxylic group to the nitrogen atom. The potential energy surface (PES) curves (Fig. 8a and b) for the

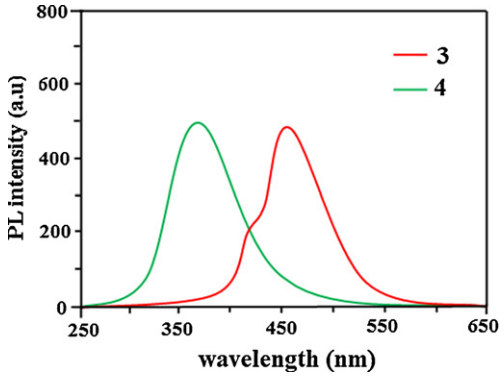

Fig. 6. Fluorescence spectra of the imidazole derivatives **3** and **4** in dioxane.

Table 3
Relative energies and dipole moment for the imidazole derivative **3**.

Rotamer	Ground state		Excited state	
	μ (D)	E (eV)	μ (D)	E (eV)
I	4.81	0.05 (0.00)	9.25	4.00 (3.52)
II	4.55	0.09 (0.03)	9.01	4.52 (4.02)
III	6.22	0.51 (0.32)	4.01	3.82 (3.00)

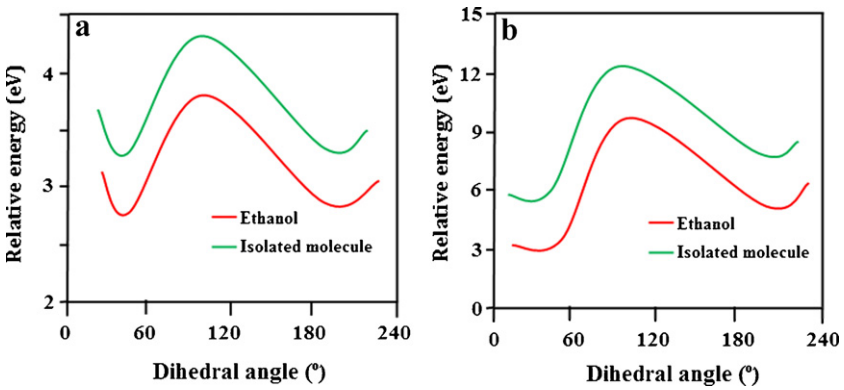

Fig. 8. The potential energy surface curves for the interconversion of isomers I and II of the imidazole derivative **3** in the ground and excited states.

interconversion of isomers I and II of **3** in the ground state for isolated molecule is 4.5 kcal/mol and that in ethanol is 3.6 kcal/mol. The corresponding value in the excited state for the isolated molecule is 12.8 kcal/mol and that in ethanol is 10.0 kcal/mol, respectively. The barrier for interconversion in the excited state is much higher than that in the ground state (Table 3).

3.4. Molecular electrostatic potential map (MEP)

In order to prove the higher electron density at N(3), we have performed DFT calculation to get the molecular electrostatic potential (MEP) for **1**–**4**. The MEP map (Fig. 9) shows that oxygen, nitrogen and fluorine atoms represent the most negative potential region (dark red). (For interpretation of the references to colour in text, the reader is referred to the web version of this article.) The nitrogen atom seems to exert comparatively small negative potential as compared to oxygen atom. The predominance of green region in the MEP surface corresponds to a potential halfway between the two extremes red and dark blue colour [21].

3.5. HOMO–LUMO energies of imidazole derivatives *1*–*4* by DFT method

The energy gap between the highest occupied molecular orbital (HOMO) and the lowest unoccupied molecular orbital (LUMO) has been used to prove the bioactivity from intramolecular charge transfer (ICT) and also reflect the chemical activity of the molecule [22]. The HOMO–LUMO energy gap (Table 4) of **1**–**4** have been calculated by B3LYP/6-31G(d,p) and from the HOMO–LUMO orbital picture (Fig. 10) it was found that the HOMO is located on the imidazole ring (not on the two phenyl rings attached to the C3 and C4 carbons of the imidazole rings) and the phenyl ring attached to the C2 carbon of the imidazole ring and the LUMO located on the imidazole ring (the two phenyl rings attached to the C3 and C4 carbons of the imidazole rings with C2 carbon). The HOMO → LUMO

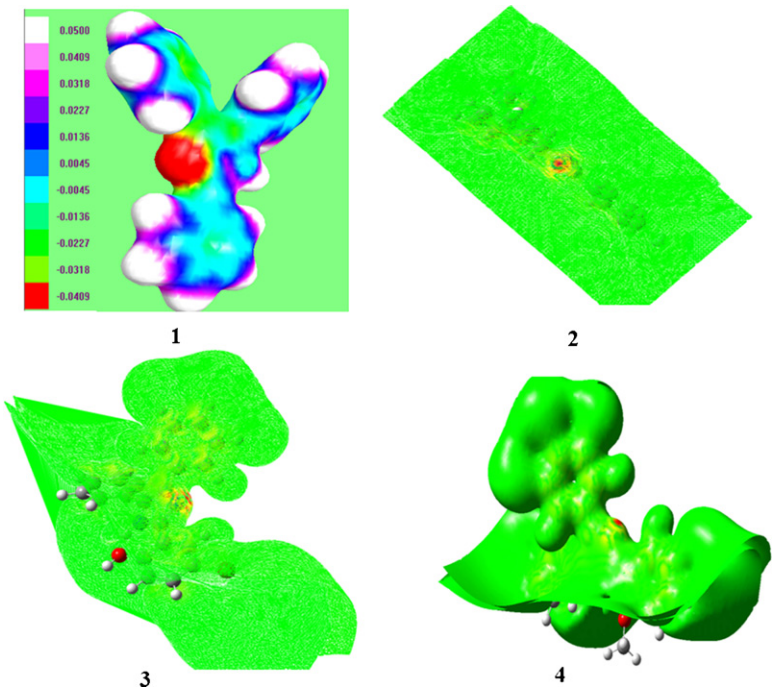

Fig. 9. MEP surface diagrams of the imidazole derivatives **1**–**4**.

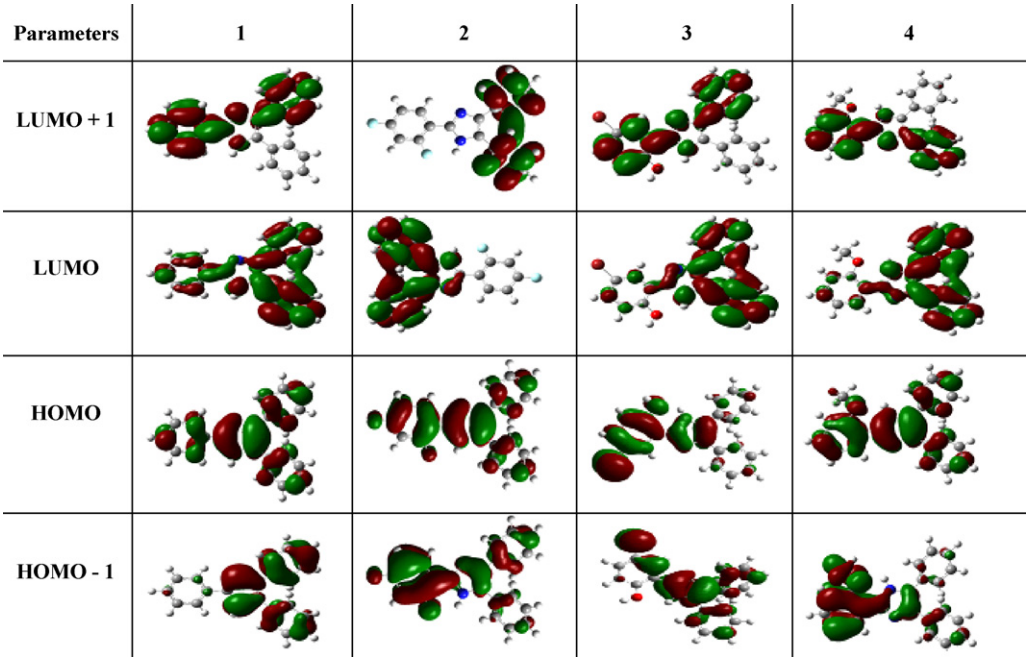

Fig. 10. HOMO–LUMO energy level diagrams of the imidazole derivatives **1–4**.

transition implies that intramolecular charge transfer takes place within the molecule [23,24].

Therefore, introduction of an electron donating substituent into the phenyl ring attached to the C2 carbon raises the energy of the HOMO resulting in a red-shift of the emission. On the other hand, the introduction of the electron withdrawing substituent into the aldehydic phenyl ring lowers the energy of the HOMO, and leads to the blue shift of the emission. The calculated energy gap explains the eventual charge transfer interactions within the molecule. The optimized HOMO−1, HOMO, LUMO and LUMO+1 molecular orbitals of **1–4** revel that HOMO−1 and HOMO have identical nodal patterns, *i.e.*, nodal between the phenyl and imidazole ring portions of the orbital. Therefore the π-interaction between two rings is anti-bonding in character. From Table 4, it was concluded that the lowest energy transition ($S_0 \rightarrow S_1$) corresponds to HOMO → LUMO transition having higher oscillator strength and the higher energy transition ($S_0 \rightarrow S_2$) corresponds to (HOMO−1 → LUMO) transition having lower oscillator strength.

3.6. Fluorescent chemosensor

Imidazole derivatives have been used to construct highly sensitive fluorescent chemosensors for sensing and imaging of metal ions and its chelates in particular those with Ir^{3+} are major components for organic light emitting diodes [26–30]. They are promising candidates for fluorescent chemosensors for metal ions such as Mn^{2+}, Pb^{2+}, Co^{2+}, Zn^{2+}, Hg^{2+} and Cu^{2+}, if their radiationless channel could be blocked by metal binding. The fluorescence enhancement was observed (Table 5) to a different extent which shows that the metal ions binding blocks the radiationless decay channel (Fig. 11). The radiative (k_r) and non-radiative (k_{nr}) rate constants have been calculated in Cu^{2+} in acetonitrile. The observed non-radiative emission (k_{nr}) may be due to n–π* transition [25]. It was found that the substantial increase in the quantum yield in the presence of Cu^{2+} is due to dramatic decrease in nonradiative transition whereas the radiative constant remains unchanged within the experimental error. That is the radiationless decay due to n–π* transition

Table 4
HOMO–LUMO energies of the imidazole derivatives **1–4**.

Compound	ϕ	HOMO−1 (eV)	HOMO (eV)	LUMO (eV)	LUMO+1 (eV)	E_g ($E_{HOMO-1} - E_{LUMO}$) (eV)	E_g ($E_{HOMO} - E_{LUMO}$) (eV)
1	0.41	−0.345	−0.301	0.001	−0.014	0.346 (0.410)	0.302 (0.505)
2	0.52	−0.348	−0.304	−0.010	−0.028	0.358 (0.201)	0.293 (0.219)
3	0.60	−0.308	−0.293	−0.193	−0.200	0.115 (0.086)	0.100 (0.268)
4	0.63	−0.334	−0.302	−0.193	−0.200	0.141 (0.001)	0.102 (0.115)

Values in the parenthesis corresponds to oscillator strength.

Table 5
Emission spectral data of **1–4** with Cu^{2+} metal ion at different concentrations.

Concentration of Cu^{2+} metal (M)	**1** λ_{emi} (nm)	**2** λ_{emi} (nm)	**3** λ_{emi} (nm)	**4** λ_{emi} (nm)
0	388.5 (440.5)	385.2 (446.7)	428.2 (363.7)	388.1 (183.6)
1×10^{-5}	420.4 (536.4)	400.7 (598.4)	448.4 (524.4)	420.5 (293.6)
5×10^{-5}	420.3 (602.4)	400.6 (618.6)	448.5 (538.5)	420.4 (296.7)
1×10^{-4}	420.5 (611.9)	400.6 (630.8)	448.2 (551.7)	420.5 (301.4)
5×10^{-4}	420.3 (622.5)	400.8 (641.7)	448.3 (566.1)	420.6 (333.8)
1×10^{-3}	420.1 (638.9)	400.7 (662.4)	448.2 (577.6)	420.3 (354.4)
5×10^{-3}	420.2 (656.6)	400.8 (675.5)	448.5 (590.5)	420.5 (369.5)

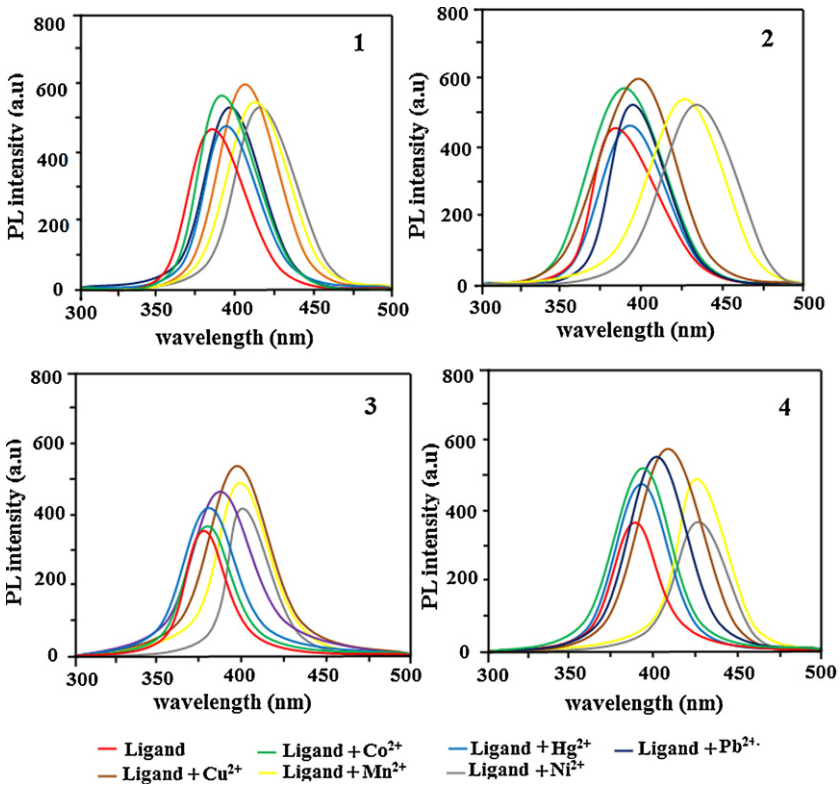

Fig. 11. Fluorescence chemisensors blocking by metal ion binding.

that is blocked upon metal binding and the emission of chelate [Cu^{2+}-ligands] originates only from π–π^* transition.

4. Conclusion

Intermolecular hydrogen bonding of hydroxy imidazole with water giving rise to IV impedes the ESIPT process, resulting in an increase in the quantum yield of normal emission at the expense of tautomer emission. Fluorescence enhancement has been found in the presence of transition metal ions. This resulted from the suppression of radiationless transitions from the n–π^* state in the chemosensors. DFT calculation supports the π-electron densities in the excited electronic state that is the driving force for the intramolecular proton transfer from the hydroxylic group to the N(3) nitrogen atom. PES calculation reveals that the barriers for interconversion in the excited state are much higher than that in the ground state. HOMO–LUMO energies and energy gap reveal the existence of intramolecular charge transfer within the molecule. MEP map supports the higher electron density at N(3) nitrogen atom.

Acknowledgments

One of the authors Dr. J. Jayabharathi, Associate professor, Department of Chemistry, Annamalai University is thankful to Department of Science and Technology [No. SR/S1/IC-07/2007] and University Grants Commission (F. No. 36-21/2008 (SR)) for providing funds to this research work.

References

[1] P.T. Chou, M.L. Martinez, J.H. Clements, J. Phys. Chem. 97 (1993) 2618–2622.
[2] F. Gai, R.L. Rich, J.W. Petrich, J. Am. Chem. Soc. 116 (1994) 735.
[3] L.F. Campo, F.S. Rodembusch, V. Stefani, J. Appl. Polym. Sci. 99 (2006) 2109–2116.
[4] Y. Wu, X. Peng, J. Fan, S. Gao, M. Tian, J. Zhao, S. Sun, J. Org. Chem. 72 (2007) 62–66.
[5] J.G. Lambardino, E.H. Wiseman, J. Med. Chem. 17 (1974) 1182–1188.
[6] T. Maier, R. Schmierer, K. Bauer, H. Bieringer, H. Buerstell, B. Sachse, US Patent 820335 (1989);
T. Maier, R. Schmierer, K. Bauer, H. Bieringer, H. Buerstell, B. Sachse, Chem. Abstr. 111 (1989) 19494.
[7] I. Lantos, W. Zhang, X. Shiu, D.S. Eggleston, J. Org. Chem. 58 (1993) 7092–7095.
[8] C. Zhang, E.J. Moran, T.F. Woiwade, K.M. Short, A.M. Mjalli, Tetrahedron Lett. 37 (1996) 751–754.
[9] S. Jianwei, Y. Dong, L. Cao, X. Wang, S. Wang, Y.Y. Hu, J. Org. Chem. 69 (2004) 8932–8934.
[10] M.J. Frisch, G.W. Trucks, H.B. Schlegel, G.E. Scuseria, M.A. Robb, J.R. Cheeseman, J.A. Montgomery, T. Vreven Jr., K.N. Kudin, J.C. Burant, J.M. Millam, S.S. Iyengar, J. Tomasi, V. Barone, B. Mennucci, M. Cossi, G. Scalmani, N. Rega, G.A. Petersson, H. Nakatsuji, M. Hada, M. Ehara, K. Toyota, R. Fukuda, J. Hasegawa, M. Ishida, T. Nakajima, Y. Honda, O. Kitao, H. Nakai, M. Klene, X. Li, J.E. Knox, P. Hratchian, J.B. Cross, C. Adamo, J. Jaramillo, R. Gomperts, R.E. Stratmann, O. Yazyev, A.J. Austin, R. Cammi, C. Pomelli, J.W. Ochterski, P.Y. Ayala, K. Morokuma, G.A. Voth, P. Salvador, J.J. Dannenberg, V.G. Zakrzewski, S. Dapprich, A.D. Daniels, M.C. Strain, O. Farkas, D.K. Malick, A.D. Rabuck, K. Raghavachari, J.B. Foresman, J.V. Ortiz, Q. Cui, A.G. Baboul, S. Clifford, J. Cioslowski, B.B. Stefanov, G. Liu, A. Liashenko, P. Piskorz, I. Komaromi, R.L. Martin, D.J. Fox, T. Keith, M.A. Al-Laham, C.Y. Peng, A. Nanayakkara, M. Challacombe, P.M.W. Gill, B. Johnson, W. Chen, M.W. Wong, C. Gonzalez, J.A. Pople, Gaussian 03, Revision C.02, Gaussian, Inc., Wallingford, CT, 2004.
[11] J. Jayabharathi, V. Thanikachalam, K. Brindha Devi, N. Srinivasan, Spectrochim. Acta A 82 (2011) 513–520.
[12] J. Jayabharathi, V. Thanikachalam, N. Srinivasan, K. Saravanan, J. Fluoresc. (2010), doi:10.1007/s10895-010-0747-5.
[13] J. Jayabharathi, V. Thanikachalam, N. Srinivasan, K. Jayamoorthy, M. Venkatesh Perumal, J. Fluoresc. 21 (2011) 1813–1823.
[14] J. Jayabharathi, V. Thanikachalam, K. Jayamoorthy, M. Venkatesh Perumal, Spectrochim. Acta A 79 (2011) 6–16.
[15] J. Jayabharathi, V. Thanikachalam, M. Venkatesh Perumal, N. Srinivasan, Spectrochim. Acta A 83 (2011) 200–206.
[16] J. Jayabharathi, V. Thanikachalam, K. Saravanan, M. Venkatesh Perumal, Spectrochim. Acta A 79 (2011) 1240–1246.
[17] K. Das, N. Sarkar, A.K. Ghosh, D. Majumdar, D.N. Nath, K. Bhattacharyya, J. Phys. Chem. 98 (1994) 9126.
[18] P.F. Barbara, P.K. Walsh, L.E. Brus, J. Phys. Chem. 93 (1989) 29–34.
[19] G.J. Woolfe, M. Melzig, S. Schneider, F. Dorr, Chem. Phys. 77 (1983) 213–221.
[20] A.L. Sobolewski, Chem. Phys. Lett. 211 (1993) 293.
[21] J. Jayabharathi, V. Thanikachalam, M. Venkatesh Perumal, N. Srinivasan, Spectrochim. Acta A 79 (2011) 236–244.

[22] J. Jayabharathi, V. Thanikachalam, M. Venkatesh Perumal, Spectrochim. Acta A 85 (2012) 31–37.
[23] Q. Sun, Z. Li, X. Zeng, M. Ge, D. Wang, J. Mol. Struct. (Theochem) 724 (2005) 167–172.
[24] S.Y. Chai, R. Zhou, Z.W. An, A. Kimura, K. Fukuho, M. Matsumura, Thin Solid Films 479 (2005) 282–287.
[25] Z. Zhou, C.J. Fahrni, J. Am. Chem. Soc. 126 (29) (2004) 8862.
[26] J. Jayabharathi, V. Thanikachalam, N. Srinivasan, M. Venkatesh Perumal, Spectrochim. Acta A 79 (2011) 338–347.
[27] J. Jayabharathi, V. Thanikachalam, N. Srinivasan, M. Venkatesh Perumal, J. Fluoresc. 21 (2011) 1585–1597.
[28] J. Jayabharathi, V. Thanikachalam, K. Saravanan, N. Srinivasan, J. Fluoresc. 21 (2010) 507–519.
[29] J. Jayabharathi, V. Thanikachalam, N. Srinivasan, M. Venkatesh Perumal, J. Fluoresc. (2010), doi:10.1007/s10895-011-0847-x.
[30] J. Jayabharathi, V. Thanikachalam, A. Saravanan, J. Photochem. Photobiol. A 208 (2009) 13–20.